

Document downloaded from:

<http://hdl.handle.net/10251/80122>

This paper must be cited as:

Mollar García, MA.; Cembrero Cil, J.; Marí, B. (2016). Photoluminescent properties of electrochemically synthesized ZnO nanotubes. *Materials Characterization*. 119:152-158. doi:10.1016/j.matchar.2016.07.022.



The final publication is available at

<http://dx.doi.org/10.1016/j.matchar.2016.07.022>

Copyright Elsevier

Additional Information

Photoluminescent properties of electrochemically synthesized ZnO nanotubes

J. M. Gracia Jiménez^a, J. Cembrero^b, M. Mollar^c, B. Mari^{c,*}

^a Instituto de Física, Benemérita Universidad Autónoma de Puebla, Apartado Postal J-48, Puebla, Pue. 72570 México

^b Departament d'Enginyeria Mecànica i Materials, Universitat Politècnica de Valencia, Camí de Vera s/n, 46071 - València, Spain

^c Departament de Física Aplicada-IDF, Universitat Politècnica de Valencia, Camí de Vera s/n, 46071 - València, Spain

* Corresponding author: bmari@fis.upv.es

Abstract

ZnO nanotubes were prepared by a sequential combination of electrochemical deposition, chemical attack and regeneration. ZnO nanocolumns were initially electrodeposited on conductive substrates and then converted into nanotubes by a process involving chemical etching and subsequent regrowth. The morphology of these ZnO nanocolumns and derived nanotubes was monitored by Scanning Electron Microscopy and their optical properties was studied by photoluminescence spectroscopy. Photoluminescence were measured as a function of temperature, from 6 to 300 K, for both nanocolumns and nanotubes. In order to study the behaviour of induced intrinsic defect all ZnO films were annealed in air at 400 °C and their photoluminescent properties were also registered before and after annealing. The behaviour of photoluminescence is explained taking into account the contribution of different point defects. A band energy diagram related to intrinsic defects was proposed to describe the behaviour of photoluminescence spectra.

Keywords: Nanocolumns; Nanotubes; Growth from solution; Zinc Oxide; Defects; Photoluminescence.

Introduction

Zinc Oxide (ZnO) is a wide gap semiconductor well known for various potential applications in low-voltage and short-wavelength optoelectronic devices, such as light emitting and laser diodes, optical windows and solar cells [1-3]. In the last few years, owing to its potential applications in ultraviolet optoelectronic devices, a growing number of research projects have been developed using ZnO as basic material. Nanostructured samples of ZnO have been prepared by many different techniques, such as plasma-assisted molecular beam epitaxy [4], chemical vapor deposition [5], and pulsed laser deposition [6]. As another approach, electrodeposition (ED) presents several advantages over the above mentioned techniques such as low temperature processing and low cost [7, 8]. This technique allows controlling nanostructure dimensions by means of the growth parameters [9].

Unintentionally doped ZnO is always is an n-type semiconductor due to the existence of defects involving O vacancies (V_O) or Zn interstitial (Zn_i), which act as donors. Theoretical calculations based on ab-initio methods support this experimental fact [a]. Owing to these defect-related donors, p-type doping is still a challenge and numerous efforts addressed to reduce this type of native defects have been carried out in the last decade. Indeed, a better understanding of their properties could pave the way for improving the control over optical and electrical properties of ZnO. Recently, a big effort has been made to reduce such defects in order to improve their properties, and several thermal annealing procedures were explored aimed to correct the deficiency of O and / or modify other native defects [11-13]. Furthermore, it was found that chemical films etching modify the surface morphology of ZnO [9], and thus some mechanism being sensitive to emission surface quality (e.g. excitons) is also expected to modify its radiative emission.

One approach deals with the exploration of annealing in air to correct the Oxygen deficiency or to modify the nature of other types of native defects. On the other hand, it has been observed that when ZnO films are exposed to a chemical attack, the surface morphology changes and subsequently the

emission mechanisms (involving excitons or deep defects), which are sensitive to surface quality, are expected to modify their radiative emission properties [14].

The low temperature synthesis of electrodeposited ZnO usually requires post annealing treatments in order to enhance optical properties of thin films and reducing native centers thus improving crystallinity [15]. Following the evolution and optimization of optical properties, several studies have been published using reducing and/or oxidizing atmospheres [16-17]. However, the interpretation of these results is controversial regarding the contribution of different defects to the photoluminescence spectra [18-20]. On the other hand, the low temperature electrodeposition of ZnO makes this technique compatible with the use of polymers for making electroluminescent hybrid devices by means of heterojunctions formed by nanocolumns of electrodeposited ZnO and a polymer as recently demonstrated by Könenkamp [21].

Photoluminescence (PL) is a non-destructive technique, which directly probes optically active centers that affect the response of ZnO thin films and their evolution with the specific treatment applied to them. In this experiment, a group of samples was synthesized under the same growing conditions with two objectives: to investigate how atmosphere and annealing temperature could improve optical properties. As the size and surface-volume ratios of the ZnO columns depend mainly on the growth parameters, such as current density, deposition rate and deposition bath temperature and they hardly influence the emission properties [9, 17], special attention was paid to obtain samples with identical morphology.

The aim of this paper is to investigate the PL properties of nanostructured ZnO films related to their morphology (nanocolumns or nanotubes) and subsequent thermal annealing. The analysis of the PL properties will be useful to shed some light on the structure of native defects in ZnO. A model based on

the energy band diagram related to deep defects in ZnO is proposed to understand the PL behaviour of such ZnO nanostructures.

Experimental

Nanocolumnar ZnO films were prepared by electrodeposition (ED) on glass substrates covered with a conductive layer of tin oxide doped with fluorine (FTO). The electrolyte used is a solution of ZnCl₂ (5×10^{-3} M) and 0.1 M of KCl in demineralized water ($\rho > 16 \text{ M}\Omega \cdot \text{cm}$) as used in previous works [9, 15]. During the ED stages, the solution was saturated with O₂ by continuous bubbling. Temperature was controlled with a thermal blanket and remained within ± 1 °C. No stirring was applied. A three-electrode cell configuration was used, KCl saturated Ag/AgCl as reference electrode and a Pt wire as counter electrode. Measured pH in the fresh electrolyte was 6.5. The potential was fixed at -0.85 V with respect to the reference electrode. Previous results show that temperature, current density and time exposure help the formation of column growth [8].

The procedure developed to fabricate hollow ZnO nanocolumns consisted of three steps: (1) column formation by electrodeposition (ED), (2) a chemical attack to produce the hollow structures and eventually (3) regeneration of the hollow nanocolumns again by ED. This last step was required just in case the second step was too aggressive giving hollow nanocolumns but very irregular in shape. Details of the procedure to deposit ZnO nanotubes can be found elsewhere [22]. After growth of both, ZnO nanocolumns and nanotubes samples were further annealed in air at 400°C.

Photoluminescence spectroscopy was performed by excitation with the 325 nm line of a He–Cd laser with an optical power of 30 mW. The setup consisted of a Jovin Yvon TRIAX monochromator coupled to a Si-CCD detector optimized for UV-VIS range. PL measurements were carried out between 6 K and room temperature. At cryogenic temperature, samples were mounted on the cold finger of a He closed cycle cryostat refrigerator and cooled down to the desired temperature.

Results and discussion

Morphology

Figure 1 shows SEM micrographs of two ZnO samples under different conditions: a) as grown nanocolumns, b) nanotubes created after chemical etching and further regrowth. Observation by means of SEM shows this deposit in form of hexagonal nanocolumns of approximately 100 nm of base and 500 nm high [18], partially oriented is the 002 direction of a hexagonal wurtzite structure as inferred from XRD spectra [8, 9]. Nanotubes obtained after chemical etching and subsequent electrochemical regrowth are identical in form, base and height. The difference consists in the fact that the inner part of the nanocolumns is no longer present after the described process. The walls of the nanotubes are about 20 nm thick and quite regular along the deposit. Figure 1 c) shows a detail of the ZnO nanotubes.

In both morphologies, nanocolumns and nanotubes, no relevant differences were appreciated in the morphology between as-grown and annealed samples.

Photoluminescence

Figures 2a and 2b show the PL spectra registered at 6, 80 and 300 K of as-grown ZnO nanocolumns and nanotubes, respectively. As can be seen, both samples show two bands, one in the region of the shallow impurities and excitons (located at 377 and 381 nm, respectively) and one related to deeper levels with two bands centered at 610 and 622 nm, respectively.

It is known that a typical spectrum of ZnO films has two characteristic peaks: a UV near-band-edge (NBE) whose peak emission is around 377 nm [19, 22, 23], and a deep-level (DL) emission, also known as green-band or red-band depending on if they are centred around 500 or 600 nm. A sharp NBE emission peak results from excitons and its position and structure is an indication of crystal quality. The green band is related to transitions involving defects and several point defects, such as oxygen vacancy

(V_O), zinc vacancy (V_{Zn}), interstitial zinc (Zn_i), interstitial oxygen (O_i) and antisite oxygen (O_{Zn}) [22,23], have been proposed as responsible for this emission in ZnO.

The rise of intensity and shift are the result of a higher concentration of defects and associated impurities related to chemical etching and subsequent regrowth. These actions generate defects located at lower energy, i.e. etching produces defects causing a deterioration of the surface and bulk quality of ZnO. Then etching, not only changes the surface morphology of the films [22], but also increases the rate of defects or impurities existing in the material generating preferentially the ones that shift PL bands towards the red. Moreover, when the temperature increases, the emission reflects the expected behaviour, i.e. the reduction of PL intensity is due to the presence of other non-radiative processes such as electron-phonon interactions, which compete with radiative recombination processes.

When both kind of films, nanocolumns and nanotubes, are annealed in air (Figs. 3 a, b) significant changes are observed in both NBE and DL regions. As already observed in the case of chemical etching, a redistribution of impurities and defect levels can be observed in both samples, which causes the dominant peak at low energy to vanish and two new lines appear. These are located at 511 nm for the nanocolumns and 512 and 642 nm for the nanotube samples, respectively. Most notably, in this region, the intensity of the new lines in the etched sample (nanotubes) is almost the same, unlike in as-grown nanocolumns and nanotubes (Fig. 2). In addition, in the nanocolumnar sample, the lowest energy PL band appears as a shoulder that is superimposed to that of 511 nm and does not form a defined band. In the NBE region, the bands of both films drastically reduce their average FWHM, and it is observed that this is the result of the superposition of several lines, some appearing as peaks and a few others as shoulders.

Thus, as seen, thermal treatment modifies the distribution and concentration of defects and impurities, dissociating some and allowing others. When nanocolumns are annealed, the broad band centred at 610 nm (Fig. 2a) narrows and shifts to lower wavelength (511 nm) (Fig. 3a). Noteworthy, the

intensity of this DL emission for annealed nanocolumns increases about one order of magnitude. Besides a shoulder at higher wavelengths is also observed. In the case of annealed nanotubes the broad band located at 622 nm (Fig. 2b) splits into two new bands with similar intensities and located at 512 and 642 nm, respectively (Fig. 3b).

Impurities or defects involved in these bands have not been fully identified yet. However, the defects and impurities associated with the first PL band dissociate or reduce their concentration allowing the appearance of the others. It is likely that type of defects or impurities which originate the 622 nm band consist of one or two levels associated with impurities or defects such as Zn vacancies [V_{Zn}], O vacancies [V_O] or Zn interstitials [Zn_i] and oxygen interstitials [O_i] [2-4], or defects composed of two complexes such as [V_O-Zn_i] [5]. As annealing in air causes the incorporation of oxygen to the material, the concentration of V_O and complexes involving V_O must be reduced. This will increase the concentration of at least isolated Zn_i , which is reflected in the appearance of the band at 512 nm, which has been associated with a donor (Zn_i) - acceptor (V_{Zn}) transition. As a preliminary conclusion it can be said that annealing improves the quality of the surface and reduces the defects and impurities in the films.

To better show the similarities and differences between PL spectra of ZnO nanocolumns and nanotubes before and after annealing, Figures 4 were plotted to compare PL spectra recorded at 6 K. Figure 4a shows the NBE region, which as mentioned involved excitons and shallow impurities. Figure 4b shows the DL region, where defects with deeper energies in the bandgap are involved. For as-grown nanocolumnar samples a vast rise of PL intensity is observed in the NBE region, which is comparable to that observed in the DL region and is higher than observed for as grown nanotubes. Furthermore, both samples, as grown nanocolumns and nanotubes (Fig 4a) show a similar shape, which comes from the superposition of several PL bands. The dominant peak of these PL spectra is located at 371 nm and the rest appears as shoulders at 370, 373 and 381 nm, while for annealed samples the main peaks are at 370 and 381 nm with a shoulder at 375 nm. This is mainly due to the annealing that reduces defects and

improves the surface quality of the samples. In these conditions excitons and recombination involving shallow defects effectively compete with other emission mechanisms.

Concerning the DL region in both cases, a split of the initial PL (located at 620-622 nm) is observed before any thermal annealing. This red-band splits into two new bands, one located at 511 nm, which can be considered a green-band and a second red-band centred at 642 nm. The difference between nanocolumns and nanotubes is that the red-band related to annealing is more intense in the case of nanotubes than for nanocolumns. This result could be expected from the shape of the red-bands in the as-grown samples because the red-band for Zn nanotubes is more intense and is more red-shifted (622 nm) than the red-band in ZnO nanocolumns (610 nm).

As mentioned above the intensity of the NBE line depends on crystal quality allowing the formation of excitons but also on other competitor mechanisms such as transitions through the DL band or through other non-radiative levels. Hence an increase of the exciton emission intensity reveals an exhaustion of the alternative recombination paths [24].

To shed light on the effect of the chemical attack, regeneration and thermal annealing a fitting procedure for all PL spectra were carried out. In the DL region the PL peaks were deconvoluted for all studied samples. Figures 5 a, b, c, d show the different components for PL spectra recorded at 6K for all the studied samples: a) nanocolumns, b) nanotubes, c) annealed nanocolumns and d) annealed nanotubes. As can be seen, the PL spectra for the as-grown nanocolumns and nanotubes consist of two overlapping emission bands centred at 583 and 656 nm for as-grown nanocolumns and 591 and 667 for regenerated nanotubes. The emission bands centred at 583 and 591 nm belong to the region known as yellow emission for ZnO [25], while bands centred at 656 and 667 nm are usually labelled as red emission [26].

The chemical etching and subsequent regeneration performed in the synthesis of nanotubes produce a red shift of about 10 nm and a narrowing of the FWHM of about 2 nm. Furthermore, the intensity of its PL bands increases about 8 times with respect to the as-grown nanocolumns (Fig. 5a and

5b). The change in the position and FWHM of PL peaks indicates a redistribution of defects, while the increase in the emission intensity is related to an increase in the density of defects. These defects are likely to be associated to the incorporation of O and Zn during the regeneration process.

On the other hand, it is generally accepted that the green emission stems from the recombination of one electron in an oxygen vacancy (V_O) with a hole coming from the valence band and the red emission is the result of the recombination of an electron in a V_O with a hole coming from a zinc vacancy (V_{Zn}). As a result, the red shift and narrowing of PL bands should correspond to these mechanisms. That means that both emission bands are associated to the same defect, V_O . Furthermore, the chemical etching modifies the surface sample until transforming nanocolumns into nanotubes and creating a high density of O and Zn vacancies near the internal surface of the nanotube. The larger number of these defects in nanotubes than in nanocolumns would explain the increase in the intensity of PL bands in the regenerated nanotubes, meaning that the regeneration does not completely recover the defects produced during the chemical etching. Therefore, the mechanisms for this radiative recombination can be assigned unambiguously to the transitions of V_O -VB and V_O - V_{Zn} . Then, the chemical etching and subsequent regeneration do not only modify the morphology of the nanocolumns but also modify the emission due to the proliferation and redistribution of vacancy related defects.

Figures 5 c) and d) display the deconvolution of the DL band for the nanocolumns and nanotubes annealed in air at 400 °C for one hour. As can be observed, in both samples the thermal annealing redistributes and increases the impurity levels in such a way that the DL bands are now the superposition of three bands. It is noteworthy to note that PL peaks in the DL region are shifted to shorter wavelengths and FWHMs are narrower for nanotubes than for nanocolumns (see Table I).

After thermal annealing, the emission of nanocolumns increases, becoming similar in intensity the emission of nanotubes. Taking into account that the sole morphological difference between both samples resides in the higher area for nanotubes than for nanocolumns, the incorporation of O during the

annealing should be more efficient for nanotubes, resulting in a reduction of V_O . This effect explains that red and green emission bands associated to V_O have narrower a FWHM and are blue-shifted with respect to nanocolumns. In addition, the difference between red bands is the result of morphological differences as in nanotubes there should be a larger amount of V_{Zn} than in nanocolumns, which remain practically unaltered with the annealing. Taking into account that the main difference between the two groups of samples, nanocolumns and nanotubes, is the higher surface in nanotubes due to the existence of both inner and outer faces than in nanocolumns, the incorporation of oxygen during the annealing should be more efficient, resulting in a decrease of V_O . The decrease of the amount of V_O produces a blue shift of the position and a narrowing of the FWHM with respect to that observed in nanocolumns. Moreover, the difference in intensity between the red lines is also the result of the morphological differences, since in nanotubes there should be a greater concentration of V_{Zn} than in nanocolumns, which remain unchanged by the annealing.

Further, the annealing generates a third line (DL3) located at lower wavelength, 496 nm for nanocolumns and 488 nm for nanotubes. As for the yellow and red lines the blue line has narrower FWHM and again is located at shorter wavelength when emitted from nanotubes than when emitted from nanocolumns. This shift to higher energies is likely due to the reduction in size in the walls of nanotubes, which have a thickness of about 20 nm. The emission line located at 496 nm has been previously reported [3,27] in Ag-doped ZnO samples, however to our knowledge the 488 nm emission line has not yet been reported. We believe that the 488 nm blue emission line should be due to the nanometric size of the walls of nanotubes.

Figure 7 shows a band diagram schema of the energy levels of involved in the photoluminescence emission of nanotubes and nanocolumns before and after thermal annealing. All radiative transitions in the called DL region have been summarized in the schema. Chemical etching and subsequent regrowth results in a shift to longer wavelengths (shorter energies). After thermal annealing additional peaks

appear, being the trend to shift to shorter wavelengths. Similar results for have been reported elsewhere [12, 13].

Furthermore, the envelope of the bands in the region NBE is formed by two lines (NBE1 and NBE2) for films independently of any chemical etching and regrowth. PL lines corresponding to the samples with etching and regeneration have energy peaks at lower energies and slightly increase in intensity and FWHM (See Table I). As in the case of deep impurity region, changes obey to redistribution and increase of energy levels associated with defects and impurities generated by the etching and regeneration in this region. Considering the average FWHM of the lines (Table I), these lines cannot be associated to excitons, because they have higher values than those reported for excitons. So its origin is associated with impurity-band transitions (FB or BF) or with donor-acceptor pair (DAP), where the levels involved should correspond to shallow defect levels.

When thermal annealing treatment is applied to nanocolumns and nanotubes films, the impurity levels or defects reduce its amount and redistribute because after deconvolution five lines are obtained. The position and FWHM of such PL lines (Table I) can be associated to transitions involving the bound exciton (NBE3 and NBE4), and the free exciton plus one or two phonon replicas (NBE5, NBE6). The zero phonon line is not observable because of the filter used. The highlight of these results is that in general PL lines emitted from nanotubes have narrower FWHM than those of columns. It is known that for excitons to be observed there should be a low concentration of impurities capable to trap them and good surface quality, which is reflected in their FWHM of this emission lines. Then it can be concluded that the thermal annealing has a greater influence on the surface quality of nanotubes compared to that of the nanocolumns.

Conclusion

ZnO nanotubes were prepared by a sequential combination of electrochemical deposition, chemical

attack and regeneration of ZnO nanocolumns deposited on polycrystalline conductive FTO covered glass. ZnO nanocolumns were initially electrodeposited on conductive substrates and then converted into nanotubes. The morphology of these ZnO nanocolumns and subsequent nanotubes were monitored by SEM and their optical properties were studied by photoluminescence spectroscopy. Photoluminescence were measured as a function of temperature, from 6 to 300 K, for both nanocolumns and nanotubes. In order to study the behaviour of induced intrinsic defect all ZnO films were annealed in air at 400 °C and their photoluminescent properties were also registered before and after annealing. The behaviour of photoluminescence is explained taking into account the contribution of different point defects. A band energy diagram related to intrinsic defects was proposed to describe the behaviour of photoluminescence. These kind of hollow nanocolumns provide a suitable pattern with very high effective surfaces to develop devices based in one-dimensional (1D) nanostructures that can be coated or filled with other thin layers, nanoparticles or organic molecules.

Acknowledgments

This work was supported by Ministerio de Economía y Competitividad (ENE2013-46624-C4-4-R) and Generalitat valenciana (Prometeus 2014/044).

References

- [1] M.H. Huang, S. Mao, H. Feick, H. Yan, Y.Y. Wu, H. Kind et al. Room-temperature ultraviolet nanowire nanolasers. *Science* 2010; 292:1897-9.
- [2] L. Grigorjeva, D. Millers, J. Grabis, C. Monty, A. Kalinko, K. Smits et al. Luminescence Properties of ZnO Nanocrystals and Ceramics. *IEEE Transactions on nuclear science* 2008;55:1551-5.
- [3] R. T. Sapkal, S. S. Shinde, A. R. Babar, A. V. Moholkar, K. Y. Rajpure, C. H. Bhosale. Preparation, structural and optical properties of nanocrystalline ZnO doped with luminescent Ag-nanoclusters, *Mater. Express*. 2012;2:64-70.
- [4] Y. Chen, H. Ko, S. Hong, T. Yao. Layer-by-layer growth of ZnO epilayer on Al₂O₃ (0001) by using a MgO buffer layer. *Appl. Phys. Lett.* 2000;76:559-61.
- [5] D.C. Reynolds, D.C. Look, B. Jogai. Optically pumped ultraviolet lasing from ZnO. *Solid State Commun.* 1999;99:873-5.
- [6] Y.R. Ryu, S. Zhu, S.W. Han, H.W. White, P.F. Miceli, H.R. Chandrasekhar. ZnSe and ZnO film growth by pulsed-laser deposition. *Appl. Surf. Sci.* 1998;127:496-9.
- [7] S. Peulon, D. Lincot. Cathodic electrodeposition from aqueous solution of dense or open-structured zinc oxide films. *Adv. Mater.* 1996;8:166-70.
- [8] J. Cembrero, M. Perales, M. Mollar, B. Marí. Obtención de columnas de ZnO. Variables a controlar (I) *Bol. Soc. Es. Ceram. V.* 2003;42:379-87.
- [9] J. Cembrero, A. Elmanouni, B. Hartiti, M. Mollar, B. Marí. Nanocolumnar ZnO films for photovoltaic applications. *Thin Solid Films* 2004;451-452:198-202.
- [10] X. Teng, H. Fan, S. Pan, C. Ye, G. Li. Abnormal photoluminescence of ZnO thin films on ITO glass. *Mater. Lett.* 2007;61:201-4.

- [11] D. Kim, G. Lee, Y. Kim. Interaction of zinc interstitial with oxygen vacancy in zinc oxide: An origin of n-type doping. *Solid State Commun.* 2012;52:1711–4.
- [12] V. Kumar, V. Kumar, S. Som, A. Yousif, N. Singh, O.O. Nwaeaborwa, A. Kapoor, H.C. Swart. Effect of annealing on the structural, morphological and photoluminescence properties of ZnO thin films prepared by spin coating. *J. Colloid. Interface Sci.* 2014;428:8-15.
- [13] J. Han, P.Q. Mantas, A.M.R. Senos. Defect chemistry and electrical characteristics of undoped and Mn-doped ZnO. *J. Eur. Ceram. Soc.* 2002;22:49-59.
- [14] J.R. Sadaf, M.Q. Israr, S. Kishwar, O.Nur, M. Willander. White Electroluminescence Using ZnO Nanotubes/GaN Heterostructure Light-Emitting Diode. *Nanoscale Res. Lett.* 2010;5-957-60.
- [15] B. Marí, M. Mollar, A. Mechkour, B. Hartiti, M. Perales, J. Cembrero. Optical properties of nanocolumnar ZnO crystals. *Microelectron. J.* 2004;35:79-82.
- [16] B. Marí, F.J. Manjón, M. Mollar, J. Cembrero, R. Gómez. Photoluminescence of thermal-annealed nanocolumnar ZnO thin films grown by electrodeposition. *Appl. Surf. Sci.* 2006;252:2826-31.
- [17] B. Marí, J. Cembrero, F.J. Manjón, M. Mollar, R. Gómez. Raman Measurements on nanocolumnar ZnO Crystals. *Phys. Stat. Solidi (a)* 2005;202:1602-5.
- [18] Q. Wang, G. Wang, J. Jie, X. Han, B. Xu, J.G. Hou. Annealing effect on optical properties of ZnO films fabricated by cathodic electrodeposition. *Thin Solid Films* 2005;492:61-65.
- [19] B. Lin, Z. Fu, Y. Jia. Green luminescence center in undoped zinc oxide films deposited on silicon substrates. *Appl. Phys. Lett.* 2001;79:943.5.
- [20] F. Leiter, H. Alves, D. Pfisterer, N.G. Romano, D.M. Hofmann, B.K. Meyer. Oxygen vacancies in ZnO. *Physica B* 2003;201:340-342.
- [21] R. Könenkamp, R.C. Word, M. Godinez. Ultraviolet electroluminescence from ZnO/polymer heterojunction light-emitting diodes. *Nano Letters* 2005;5: 2005-8.
- [22] J. Cembrero, D. Busquets-Mataix, E. Rayón, M. Pascual, M. A. Pérez Puig, B. Marí. Control parameters on the fabrication of ZnO hollow nanocolumns. *Mat. Sci. Semicon. Proc.* 2013;16:211-6.

- [23] J. Lim, K. Shin, H.W. Kim, C. Lee. Effect of annealing on the photoluminescence characteristics of ZnO thin films grown on the sapphire substrate by atomic layer epitaxy. *Mat. Sci. Eng. B* 2004;107: 301-4.
- [24] J.A. Sans, A. Segura, M. Mollar, B. Marí. Optical properties of thin films of ZnO prepared by pulsed laser deposition. *Thin Solid Films* 2004;453:251-5.
- [25] H. Morkoç, U. Özgür, Zinc Oxide. Fundamentals, Materials and Device Technology. Wiley-VCH; 2009.
- [26] Bin Zhao, Ming-Ming Jiang, Dong-Xu Zhao, Yang Li, Fei Wang, De-Zhen Shen. Electrically driven plasmon mediated energy transfer between ZnO microwires and Au nanoparticles. *Nanoscale* 2015;7:1081-9.
- [27] M. A. Myers, V. Khranovsky, J. Jian, J. H. Lee, H. Wang, H. Wang. Photoluminescence study of p-type versus n-type Ag-doped ZnO films. *J. Appl. Phys.* 2015;118:065702.

Figure captions

Figure 1. SEM images of electrodeposited ZnO nanostructures: a) As deposited ZnO nanocolumns, b) ZnO nanotubes after etching and regrowth, c) detail of nanotubes showing the thickness of the wall.

Figure 2. Photoluminescence spectra of as grown electrodeposited ZnO nanostructures: a) As deposited ZnO nanocolumns, b) ZnO nanotubes after etching and regrowth of ZnO nanocolumns.

Figure 3. Photoluminescence spectra of electrodeposited ZnO nanostructures after thermal annealing: a) Nanocolumns, b) Nanotubes.

Figure 4. Comparison of photoluminescence spectra recorded at 6 K before and after annealing for ZnO nanostructures: a) Excitonic part (NBE region), b) Deep levels (DL region)

Figure 5. Fit of PL spectra in the DL region recorded at 6K for all samples studied in this work. a) Nanocolumns, b) Nanotubes, c) annealed nanocolumns, d) annealed nanotubes.

Figure 6. Fit of PL spectra in the NBE region recorded at 6K for the annealed nanotubes.

Figure 7. Band diagram schema to model the energy levels involved defects in radiative transition in the called DL region. CE and TA stand for Chemical Etching and Thermal Annealing, respectively.

FIGURES

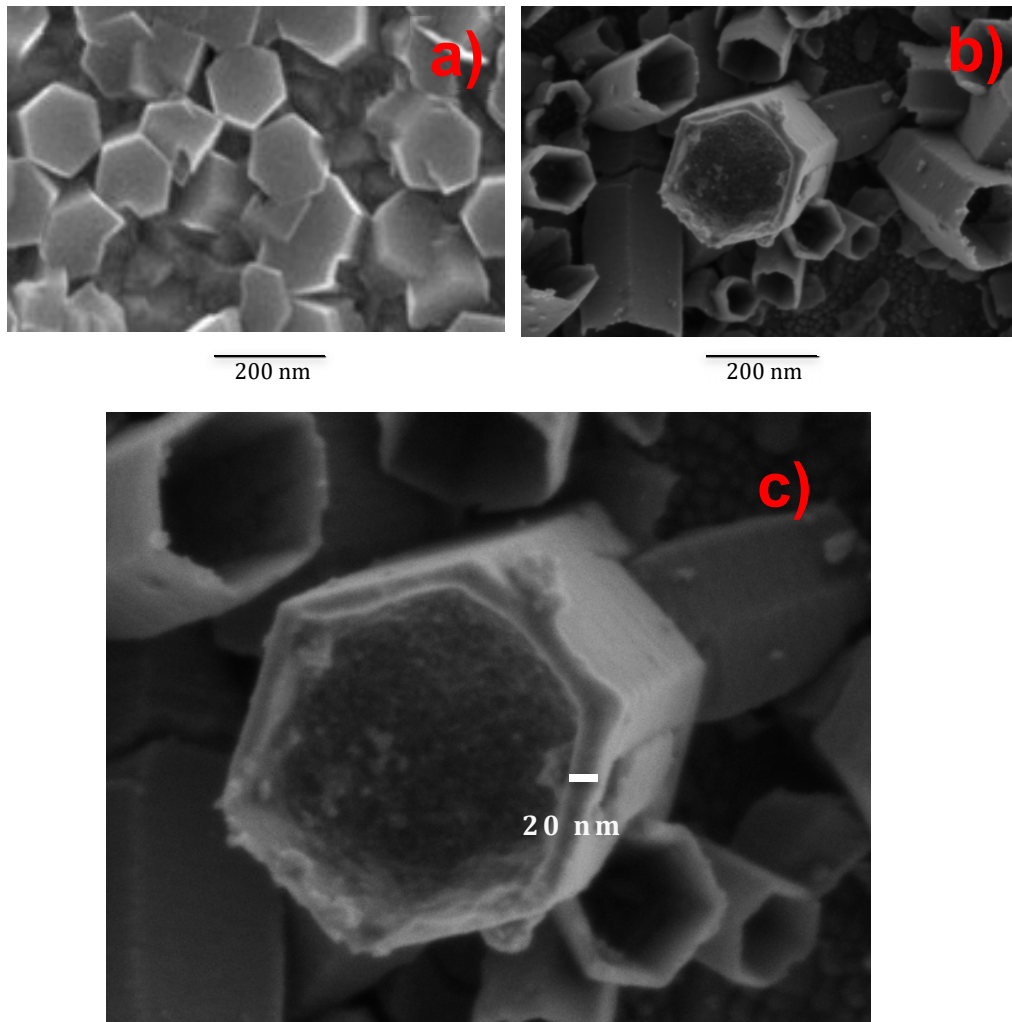


Figure 1. SEM images of electrodeposited ZnO nanostructures: a) As deposited ZnO nanocolumns, b) ZnO nanotubes after etching and regrowth, c) detail of nanotubes showing the thickness of the wall.

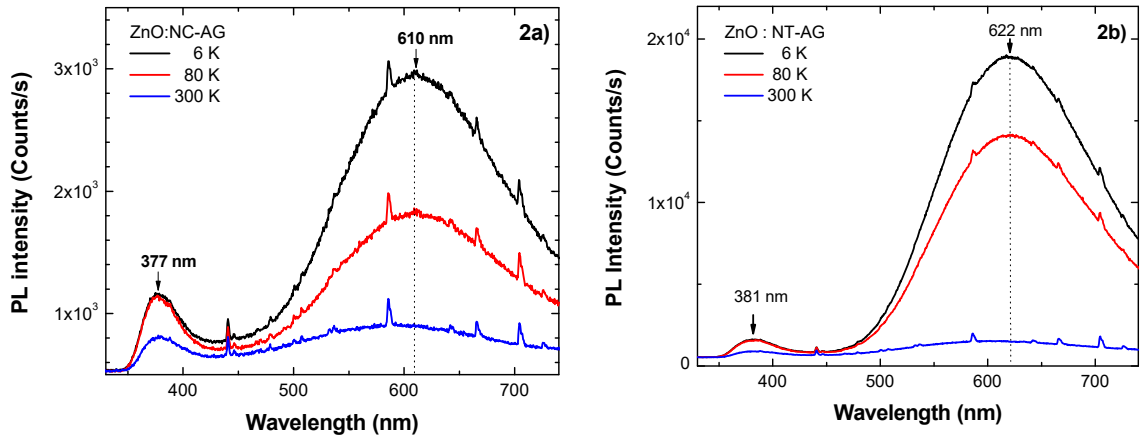


Figure 2. Photoluminescence spectra of as grown electrodeposited ZnO nanostructures: a) As deposited ZnO nanocolumns, b) ZnO nanotubes after etching and regrowth of ZnO nanocolumns.

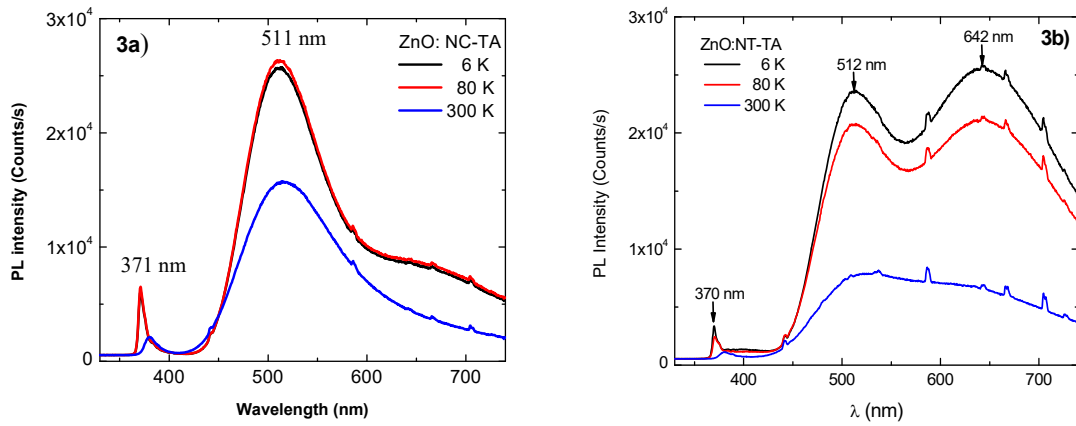


Figure 3. Photoluminescence spectra of electrodeposited ZnO nanostructures after thermal annealing: a) Nanocolumns (NC-TA), b) Nanotubes (NT-TA).

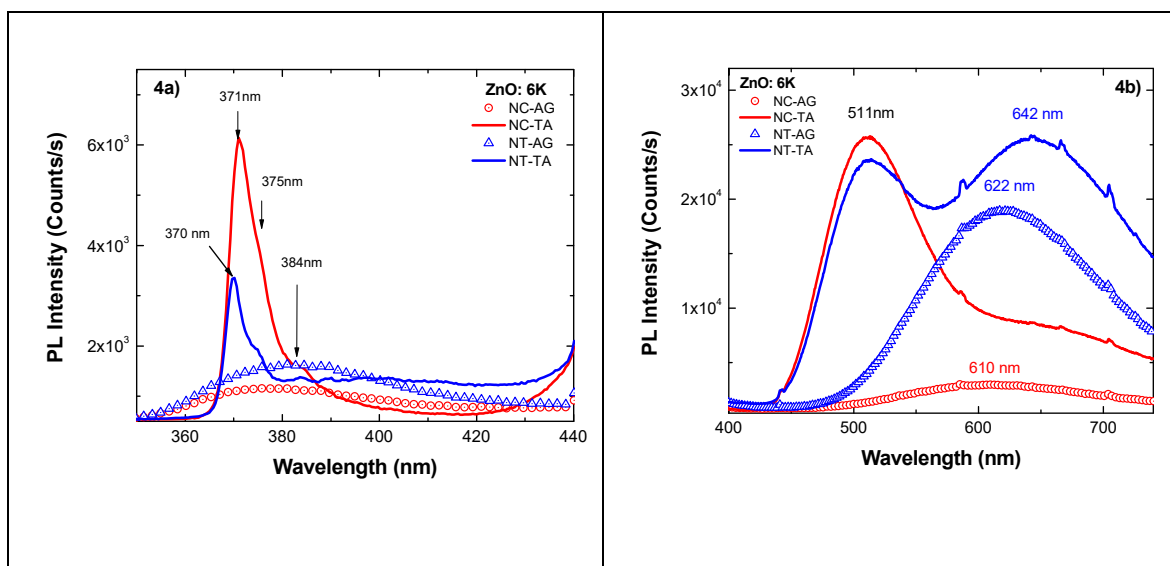


Figure 4. Comparison of photoluminescence spectra recorded at 6 K before and after annealing for ZnO nanostructures: a) Excitonic part (NBE region), b) Deep levels (DL region)

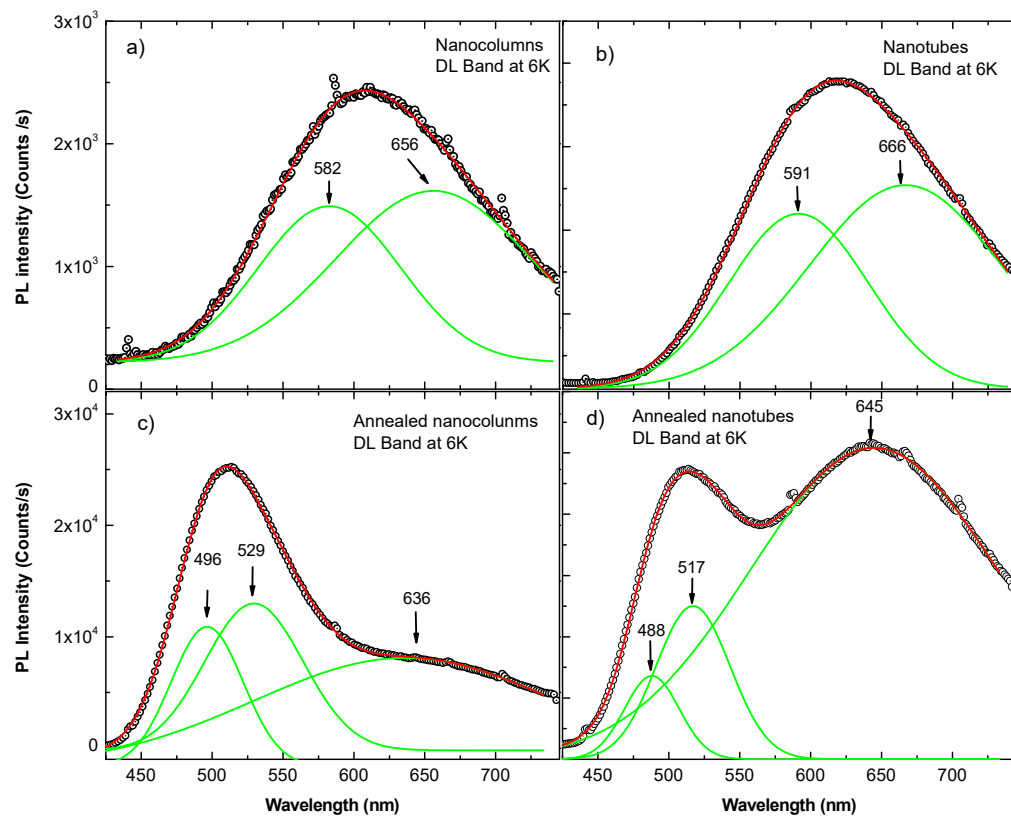


FIGURE 5. Fit of PL spectra in the DL region recorded at 6K for all samples studied in this work. a) Nanocolumns, b) Nanotubes, c) annealed nanocolumns, d) annealed nanotubes.

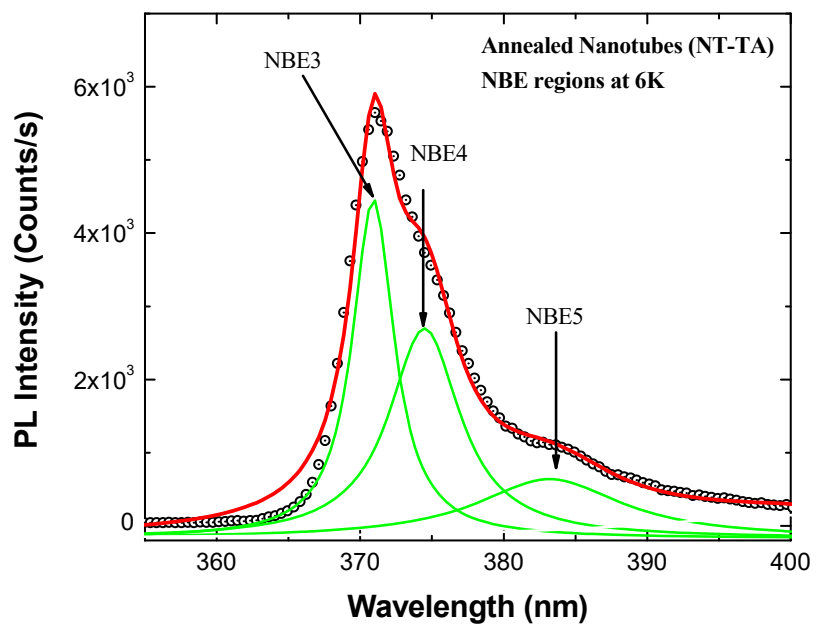


Figure 6. Fit of PL spectra in the NBE region recorded at 6K for the annealed nanotubes.

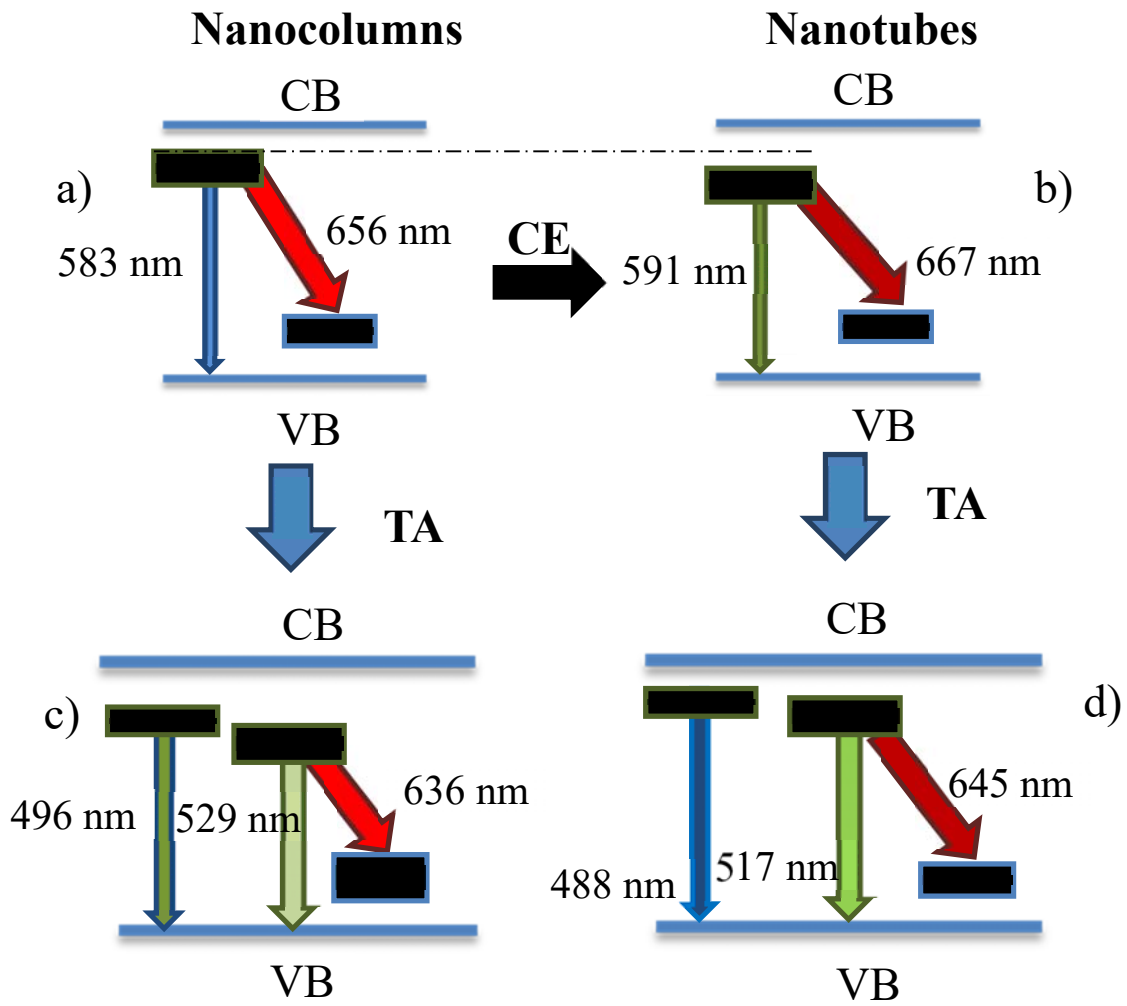


Figure 7. Band diagram schema to model the energy levels of involved defects in radiative transition in the DL region. CE and TA stand for Chemical Etching and Thermal Annealing, respectively.